2014

Arising applications of ferroelectric materials in photovoltaic devices

Yongbo Yuan
University of Nebraska-Lincoln, yyuan2@unl.edu

Zhengguo Xiao
University of Nebraska–Lincoln, zg.xiao1@gmail.com

Bin Yang
University of Nebraska–Lincoln, byang2@unl.edu

Jinsong Huang
University of Nebraska-Lincoln, jhuang@unc.edu

Journal of Materials Chemistry A

FEATURE ARTICLE

View Article Online
View Journal | View Issue

Arising applications of ferroelectric materials in photovoltaic devices

Cite this: *J. Mater. Chem. A*, 2014, **2**, 6027

Yongbo Yuan,† Zhengguo Xiao,† Bin Yang† and Jinsong Huang†*

Received 18th October 2013
Accepted 13th November 2013

DOI: 10.1039/c3ta14188h

www.rsc.org/MaterialsA

The ferroelectric-photovoltaic (FE-PV) device, in which a homogeneous ferroelectric material is used as a light absorbing layer, has been investigated during the past several decades with numerous ferroelectric oxides. The FE-PV effect is distinctly different from the typical photovoltaic (PV) effect in semiconductor p–n junctions in that the polarization electric field is the driving force for the photocurrent in FE-PV devices. In addition, the anomalous photovoltaic effect, in which the voltage output along the polarization direction can be significantly larger than the bandgap of the ferroelectric materials, has been frequently observed in FE-PV devices. However, a big challenge faced by the FE-PV devices is the very low photocurrent output. The research interest in FE-PV devices has been re-spurred by the recent discovery of above-bandgap photovoltage in materials with ferroelectric domain walls, electric switchable diodes and photovoltaic effects, tip-enhanced photovoltaic effects at the nanoscale, and new low-bandgap ferroelectric materials and device design. In this feature article, we reviewed the advance in understanding the mechanisms of the ferroelectric photovoltaic effects and recent progress in improving the photovoltaic device performance, including the emerging approaches of integrating the ferroelectric materials into organic heterojunction photovoltaic devices for very high efficiency PV devices.

1. Introduction to ferroelectric photovoltaic devices

Clean and sustainable solar energy is regarded as one of the most reliable and abundant energy sources to replace fossil fuels.[1,2] The photovoltaic effect is used to directly harvest solar energy by converting the incident photons into flowing free charge carriers and thus produce electricity. The photovoltaic technologies have advanced for more than a century after the discovery of the photoelectric effect by Einstein.[3,4] However, after decades of development, the commercialized crystalline silicon solar panels are still too expensive to compete with fossil energy.[5] In order to reduce the energy harvesting cost, the second and third generation photovoltaic cells, such as thin film amorphous silicon solar cells,[6] copper indium gallium selenide solar cells,[7] dye-sensitized solar cells,[8] cadmium telluride solar cells,[9] quantum dot solar cells,[10] organic solar

Department of Mechanical and Materials Engineering, Nebraska Center for Materials and Nanoscience, University of Nebraska, Lincoln, Nebraska 68588-0656, USA. E-mail: jhuang2@unl.edu

† All authors contributed equally.

Yongbo Yuan received his PhD degree in condensed matter physics from Sun Yat-sen University (China) in 2009, during which his research focused on organic light-emitting devices. He is currently a postdoctoral fellow in Prof. Jinsong Huang's research group at the University of Nebraska-Lincoln. His research interests include organic optoelectronics such as solar cells, thin film transistors and photodetectors.

Zhengguo Xiao obtained his B.S. at Shandong University of Science and Technology in 2008, and M.S. at the Chinese Academy of Science in 2011. Thereafter, he joined Prof. Jinsong Huang's research group in the Department of Mechanical and Materials Engineering at the University of Nebraska-Lincoln at 2011 as a PhD student. His current research focuses on organic electronic devices including OPVs, OLED, OFETs, etc.

cells,[11] perovskite solar cells,[12–14] *etc.* are under intense study because of their potential to dramatically reduce the cost by the lower-cost materials and fabrication. The power conversion efficiency (PCE, η) of a solar cell, defined by the electric energy output (P_{out}) divided by the solar energy (P_{in}) it absorbs, is expressed as:

$$\eta = P_{out}/P_{in} = J_{sc}V_{oc}FF/P_{in} \quad (1)$$

where J_{sc} is the short circuit current density, V_{oc} is the open circuit voltage, and FF is the fill factor which is the ratio of maximum obtainable power to the product of the V_{oc} and J_{sc}.

The ferroelectric photovoltaic effect was discovered about half a century ago in a variety of ferroelectric materials without central symmetry in which a steady photovoltaic response (photovoltage and photocurrent) can be generated along the polarization direction.[15,16] Generally, the ferroelectric photovoltaic effect originates from the spontaneous electric polarization in ferroelectric materials.[17,18] An unique characteristic of FE-PV devices is that the photocurrent direction can be switched by changing the spontaneous polarization direction of a FE material with the electric field. To date, the photovoltaic effect has been studied in the lithium niobate ($LiNbO_3$) family,[19–24] barium titanate ($BaTiO_3$ or referred to as BTO),[20] lead zirconate titanate ($Pb(ZrTi)O_3$ or PZT) family,[25–28] and bismuth ferrite ($BiFeO_3$ or BFO) family.[29–32]

Among the next generation photovoltaic technologies, the ferroelectric photovoltaic effect is completely different from the traditional p–n junction photovoltaic effect as shown in Fig. 1a and b. In traditional p–n junction solar cells (Fig. 1a), the absorbed photons can pump the electrons from the valence band of a light absorbing semiconductor material to its conduction band, with holes left in the valence band. The photogenerated electrons and holes are quickly separated by the built-in electric field inside the p–n junction and collected by the respective electrodes.[3] Theoretically, the magnitude of V_{oc} in p–n junction solar cells is determined by the quasi-Fermi energy difference of photogenerated electrons and holes which is limited by the bandgap of the light absorbing semiconductors.[3] Nevertheless, for the FE-PV devices (Fig. 1b), it is experimentally observed that the output photovoltage is proportional to the magnitude of electric polarization and electrode spacing.[17,18,30] As a result, a unique and important characteristic of the FE-PV devices is the anomalous photovoltaic (APV) effect, *i.e.* the output V_{oc} can be a few orders of magnitude larger than the bandgap of the FE materials.[20,21,30,33,34] The photovoltage is as large as over 10^4 volts in some cases, *e.g.* in $LiNbO_3$ bulk crystals.[33] This unique FE-PV device working mechanism provides another viable route to convert light into electric energy.

However, long after its discovery, the FE-PV effect has remained an academic curiosity rather than having any realistic application because of the very low energy conversion efficiency achieved in regular FE-PV devices. The PCE of FE-PV devices based on the pure APV effect had not exceeded 0.1% under 1 sun illumination over half a century, mainly due to very small output photocurrent densities in the order of $\sim$nA cm^{-2}.[29,35–37] The situation has not changed until recent advance in much better engineered ferroelectric materials,[30,36] new photocurrent extraction techniques,[35,38,39] and particularly the hybridization of FE-PV devices with traditional p–n junction photovoltaics which have yielded comparable or superior device performances to regular p–n junction devices.[40,41]

In this feature article, we first review the advance in understanding the mechanism of FE-PV devices, especially the origin of the abnormally large photovoltage, as well as the factors that determine the photocurrent. Then, the recent progress in enhancing the efficiency of FE-PV devices is discussed which addresses the issues of the absent and/or weak visible light absorption and low conductivity of common ferroelectric materials. And finally, the most recent advance in the application of ferroelectric materials in high efficiency organic photovoltaic (OPV) devices is highlighted. In addition to photovoltaic devices, large bandgap ferroelectric semiconductors (*e.g.* PZT and $BaTiO_3$) have also been used to separate the photogenerated charge pairs in other solar energy conversion devices, such as photoelectrochemical cells, which can be found in review papers by Tiwari *et al.* and will not be reviewed here.[42–45]

Bin Yang has been a PhD student in Prof. Jinsong Huang's research group in the Department of Mechanical and Materials Engineering at the University of Nebraska-Lincoln since 2010. He obtained a B.S. in 2007 and a M.S. in 2010 at Hunan University (China). His current research focuses on organic optoelectronic electronics.

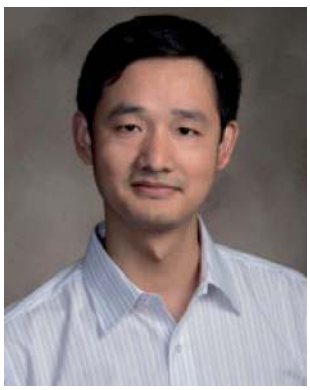

Jinsong Huang received his PhD degree in Material Science and Engineering from the University of California-Los Angeles in 2007. After working in Agiltron Inc. as a research scientist for two years, he joined the University of Nebraska-Lincoln (UNL) as an assistant professor in the Department of Mechanical Engineering and Nebraska Center for Materials and Nanoscience. His current research interests include solution processed electronic materials for applications in sensing, energy and consumer electronics.

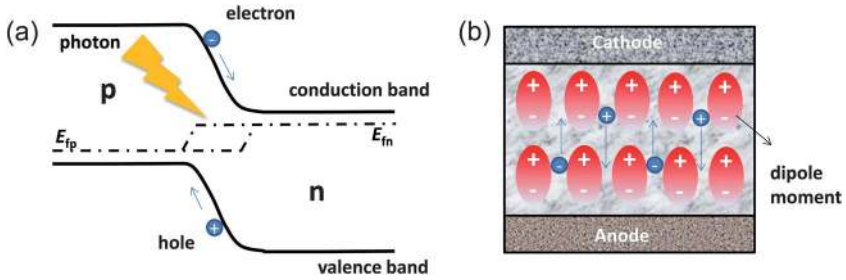

Fig. 1 The working principle of (a) p–n junction solar cells and (b) FE-PV devices.

2. Advance in the understanding of the ferroelectric photovoltaic mechanism and enhanced performance

2.1 Origin of the large photovoltage in FE-PV devices

It has been controversial on the origin of the APV effect in the ferroelectric materials. The typical FE-PV devices with vertical or lateral configurations are illustrated in Fig. 2. The photovoltage has been shown to be dependent on many factors such as the distance between the two opposite electrodes,[28,46] light intensity,[47] electrical conductivity[33] remnant polarization of the ferroelectric crystals/films,[48] crystallographic orientation,[49] dimension/size of the crystals,[46,50] domain walls[30] and the ferroelectric/electrode interface.[37] In order to explain the ultra-high photovoltage output, several models have been proposed in early years, including the shift current model and the nonlinear dielectric model.[51] The common characteristic of these theories is that the photovoltage is generated in the bulk of the ferroelectric crystals, hence named as the bulk photovoltage effect. A recent theory gives an alternative explanation on the origin of the APV effect using a series of domain walls in tandem with each other outputting a small photovoltage.[30] Other effects related to the ferroelectric/electrode interface, *e.g.* Schottky effect and screening effect,[52–55] are also believed to generate or influence the photovoltage output in ferroelectric thin films. These theories are related to the domain wall interface or the FE/electrode interface.

2.1.1 Bulk photovoltaic effect. According to the frequently cited shift current model, the ferroelectric materials act as a sort of "current-source".[21,33,34,56] The formation of a steady current (J_s) under illumination is related to the noncentrosymmetric nature of the ferroelectric crystal.[1–5,8] In the noncentrosymmetric crystal, the transition probability of an electron jump from the state with a momentum of k to the state with a momentum of k' may be different with the corresponding probability of the reverse process, which causes an asymmetric momentum distribution of the photogenerated charge carriers and thus a steady photocurrent.[17] The total current through the ferroelectric materials (J) can be described as:

$$J = J_s + (\sigma_d + \sigma_{ph})E \quad (2)$$

where σ_d and σ_{ph} are the dark conductivity and photoconductivity of the ferroelectric materials, respectively, and $E = V/d$ is the internal electric field, depending on the applied voltage (V) and the distance (d) between two electrodes. The FE-PV devices can be deemed as the current source due to the very low dark conductivity and photoconductivity[50] of most ferroelectric materials and the large distance between the electrodes.[28] The V_{oc}, corresponding to the condition of $J = 0$, can be described as:

$$V_{oc} = Ed = \frac{J_s}{\sigma_d + \sigma_{ph}} d \quad (3)$$

The shift current model predicts a larger V_{oc} under stronger light intensity I_{op} because it gives a large J_s. V_{oc} is expected to increase linearly with I_{op} (or J_s) if the total conductivity ($\sigma_d + \sigma_{ph}$) is insensitive to light intensity. This occurs in a situation where σ_{ph} is significantly lower than σ_d in the studied light intensity range. A good example for this case is the FE-PV effect in the $LiNbO_3$: Fe crystal, in which the V_{oc} increased linearly to 10^3 to 10^4 V with the light intensity in a range of 0.01–1 W cm^{-2}.[33] On the other hand, if the σ_{ph} is much larger than σ_d in the studied light intensity range, a constant V_{oc} is expected since both J_s and photoconductivity σ_{ph} are correlated with light intensity. An example for this case is that a saturated photovoltage was observed in the iron-doped potassium niobate ($KNbO_3$: Fe) crystal. Since $KNbO_3$: Fe and $LiNbO_3$: Fe have a similar crystal structure, the difference in the magnitude of σ_{ph} is related to the much longer lifetime of the photogenerated charges in $KNbO_3$: Fe.[22,33]

In the nonlinear dielectric model, the large observed photovoltage output is caused by the nonlinear response of the polarization density to the electric field of the incident light, which led to an effective DC electric field throughout the ferroelectric materials.[51]

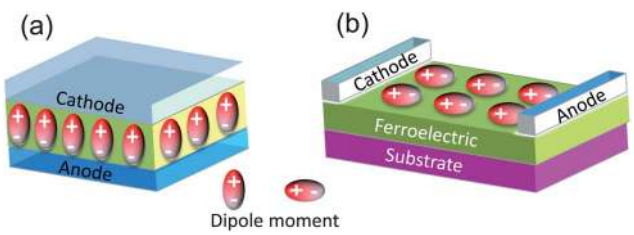

Fig. 2 FE-PV device architectures: (a) vertical and (b) lateral, in which a large photovoltage proportional to the electrode spacing can be measured along the polarization direction (P).

2.1.2 Domain wall theory. Recently, Yang *et al.* studied the APV effect on the BFO film with ordered domain strips and lateral device configuration (Fig. 3). They observed that the photovoltage in the $BiFeO_3$ film increased linearly with the total number of domain walls along the net polarization direction (perpendicular to the domain walls, Fig. 3a and c).[30] The photovoltaic effect vanished along the direction perpendicular to the net polarization direction (Fig. 3b and d). The intrinsic potential drop at domain walls (~10 mV), arising from the component of the polarization perpendicular to the domain wall, induces a huge electric field of $\sim 5 \times 10^6$ V m^{-1} in the narrow domain wall, which was suggested to be the driving force for the dissociation of the photogenerated exciton. The illuminated domain walls act as nanoscale photovoltage generators connected in series, wherein the generated photocurrent is continuous and the photogenerated voltage accumulates along the net polarization direction. This proposed mechanism is analogous to the concept of tandem solar cells, where the output voltage is the sum of the photovoltage of each sub-cell. Nevertheless, it was noticed in another publication that the domain wall is also considered as a current source, and the total V_{oc} was determined by the J_{sc}, the conductivity of the FE film under illumination and the distance between the electrodes (eqn (3)).[57] This explanation attributed the APV effect to the exciton generated inside the domain wall and suggested that the bulk photovoltaic effect was ignorable due to a quick recombination of excitons generated outside the domain wall, which is apparently different from those previously reported.[21,33,34,51,56] In contrast, it was suggested by Alexe *et al.* that the recombination of the excitons in the bulk of the BFO domain is not as quick as expected.[38] The authors investigated the BFO single crystal with a photoelectric atomic force microscopy (Ph-AFM) system combining with piezoresponse atomic force microscopy (PFM), where both the polarization direction and photocurrent can be mapped with the same scanning conducting tip. A similar large photocurrent in the regions inside or outside the domain wall was observed, indicating a weak recombination of the photogenerated carriers in the bulk of the domains. Later the lifetime of photogenerated charges in bulk BFO was measured to be as long as 75 μs which is comparable with that near the domain wall.[58]

There are other facts that cannot be explained solely by the domain wall theory and that bulk photovoltaic effect theory cannot be excluded. According to the domain wall model, the photocurrent should be independent of the light polarization directions due to the intrinsic potential drop at the domain wall induced by the polarization charges. However, the dependence of the photovoltaic current on the polarization direction of the incident light in BFO has been frequently observed,[29,31] indicating that the origin of the photovoltaic effect in ferroelectrics is more complex than expected. A first-principle calculation based on the bulk photovoltaic effect tried to reconcile the contradictory observations in the BFO devices.[59] It was explained that the vanished photocurrent along the direction parallel to the striped domain wall in Yang's experiment is mainly attributed to the unique geometry of the striped domains, where the bulk photovoltaic effect in each domain was cancelled by the adjacent domains. It was also pointed out that the large observed photovoltage in Yang's experiment should be attributed to the domain wall effect because it formed a photocurrent in the opposite direction with that of the bulk effect. This study also indicates that the photocurrent due to the domain wall effect was partially cancelled by the bulk effect. An enhanced PCE is hence expected if the photovoltaic currents caused by the bulk photovoltaic effect and domain wall effect can be designed to be in a same direction.[59]

2.1.3 Schottky-junction effect. When the ferroelectric semiconductors form Schottky contacts with metal electrodes, there is photocurrent under illumination driven by the local electrical field which is caused by the band bending near the electrodes. The generated photocurrent is largely determined by the Schottky barrier height and the depletion region depth.[60] The magnitude of the photovoltage caused by the Schottky contact is still limited to the bandgap of the ferroelectric semiconductor materials. The photovoltage caused by the Schottky-junction effect was ignored in the early stage of studies

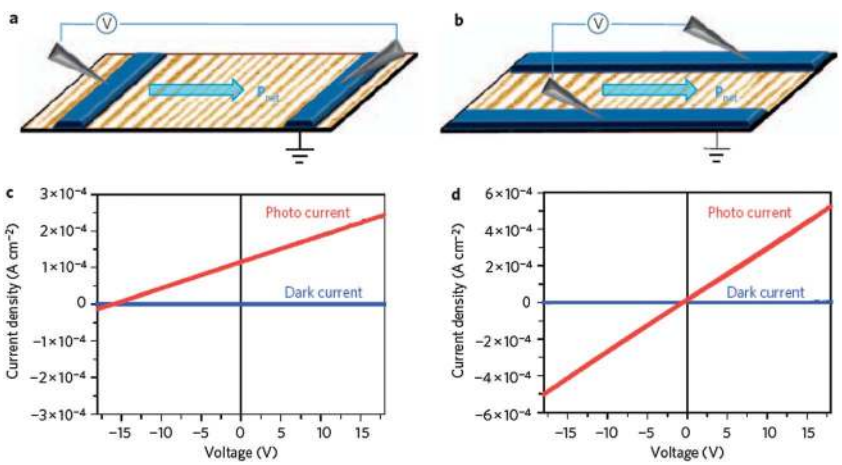

Fig. 3 Schematics of the FE-OPV device with (a) a perpendicular domain wall and (b) a parallel domain wall as demonstrated by Yang *et al.*[30] The corresponding photocurrent–voltage curves for the devices in (a) and (b) are shown in (c) and (d), respectively.

because it is much less than the anomalous photovoltage in bulk ferroelectric crystals. This effect becomes more evident in thin film FE-PV devices because of the small photovoltage output in these devices.[52,53] Generally, this additional photocurrent contribution is absent in the FE-PV devices with the same electrode contacts, because the photovoltage from the two Schottky-junctions possess opposite polarization and thus cancel each other. However, this component may play an important role in the FE-PV device with a vertical structure where different electrodes are easier to be implemented.[37,61–65] The Schottky-junction effect is independent of the polarization directions of the ferroelectric materials, which was used to distinguish the contributions of the Schottky barrier and bulk photovoltaic effects.[66] However, there are situations where the photovoltage of the Schottky-junction FE-PV devices switch together with the flip of spontaneous polarization by the applied electric bias, which often originates from some artifact effects. For example, in reported ferroelectric diodes with a vertical structure of gold (Au)/BFO/Au, a rectified dark current and photovoltage with good switch capability (between about +1 V and −1 V) were observed.[29,62] It was originally thought that the switchable photovoltage was caused by the bulk photovoltaic effect in the BFO film, but a continued study by the same group revealed that the BFO/Au contacts switched between Schottky-contact and Ohmic-contact during the poling process due to the electromigration of the oxygen vacancies, whereas the photovoltaic effect was not switched when the oxygen vacancy migration was frozen at cryogenic-temperature.[62]

2.1.4 Depolarization field model. In polarized ferroelectric films, there are high densities of polarization charges on the surface, which can induce a huge electric field inside the ferroelectric layer if they are not screened. For the BFO with a remnant polarization of 26 μC cm^{-2}, the induced electric field by the unscreened polarization charges can be as large as 3×10^4 V μm^{-1}.[67] When ferroelectric thin films are in contact with metal or semiconductors, the surface charge caused by the remnant polarization will be imperfectly screened by the free charges in the metal or semiconductors. Usually the screening of the surface charge is incomplete because the center of gravity of the polarization charge and the free compensation charge are not coincident, which results in an electrical field throughout the ferroelectric film named as the depolarization field.[68–70] This depolarization field can be large, *e.g.* the depolarization field in the 10–30 nm BTO film sandwiched between $SrRuO_3$ electrodes was estimated to be 25–50 V μm^{-1}.[71] It is suggested that the depolarization field may be the dominating driving force for the separation of photogenerated charge carrier-pairs. It was also suggested that the anomalous photovoltage should be closely related to the degree of screening of the spontaneous polarization.[35,72–74] The screening charge distribution depends on both the properties of ferroelectric materials and the metal or semiconductor, such as the remnant polarization, the free charge density and the dielectric constant. Meanwhile the impact of the incomplete screening on the depolarization field depends on the thickness of the ferroelectric layer: a smaller thickness of the ferroelectric layer results in a larger depolarization field.[46,68–70] In general, semiconductors in contact with ferroelectrics lead to a larger depolarization field than metal because of a weaker screening effect caused by their lower free charge densities and larger dielectric constants.

Recently, Dong *et al.* used aluminum-doped zinc oxide (Al : ZnO) as an electrode material, in which a larger photovoltage by about 0.25 V was found as compared to that of devices with the Au electrode. A larger depolarization electric field was suggested as one of the reasons for the increased photovoltage.[74] Chen *et al.* studied the FE-PV effect of a 400 nm-thick PZT film sandwiched between two transparent indium tin oxide (ITO) layers. The ITO films were used as electrodes because a large depolarization field was expected. They observed a gradually decreased photovoltage output from 0.4 V to 0.1 V and attributed it to a reduced depolarization field in the PZT film caused by different remnant polarizations.[73,74] The tunable screening effect provides opportunities to verify if the depolarization field has a critical contribution to the APV. However, the relationship of the depolarization field and the photovoltage output in the previous reports were not clearly revealed due to the presence of some other mechanism such as different built-in potential or changed remnant polarization.[73,74] On the other hand, it has been observed that the influence of the depolarization field on the photocurrent is stronger than on the photovoltage, where tens of times improvement in the photocurrent was reported experimentally and computationally, as will be discussed below.[35,72]

Since the depolarization field is inversely proportional to the distance between the two electrodes, the depolarization field can play a role in the photovoltaic response only when the ferroelectric films are thin (<100 nm) but it will be too low to account for the photovoltaic effect in bulk ferroelectric crystals (>100 μm).[46,68–70]

2.2 Factors determining the photocurrent in FE-PV devices

In contrast to the huge photovoltage output, the photocurrents of the FE-PV device are quite low, usually in the order of nA cm^{-2}.[17] The photocurrent of the FE-PV device is determined by the light absorption process, dissociation efficiency of the excitons, lifetime of the photogenerated nonequilibrium charges and the charge carrier mobility. The photocurrent under a certain wavelength light illumination was described by an empirical equation called Glass law: $J_s = \alpha\kappa I_{op}$, where α is the absorption coefficient, κ is the Glass coefficient which is related to the charge generation and collection efficiency and I_{op} is the light intensity as mentioned above.[21]

2.2.1 Optical bandgap and absorption coefficient. Similar to any type of photovoltaic device, the ferroelectric materials should be able to absorb as much sun light as possible to have a reasonably large photocurrent, which requires the ferroelectric materials to have a low bandgap and large absorption coefficient. Most of the commonly used ferroelectric materials, such as $LiNbO_3$, $BaTiO_3$, and PZT crystal, have a bandgap larger than 3 eV, thus can only harvest sunlight in the UV range. However, the total energy of the light with a wavelength less than 400 nm constitutes only about 3.5% of solar energy. Hence it is crucial to develop ferroelectric materials with a reduced bandgap. Recently

BFO has attracted intensive research interest for optoelectronics application because of its lower bandgap.[29,31,36,55,62,74–80] The bandgaps of its rhombohedral single crystal, rhombohedral polycrystalline,[75,76] and pseudocubic perovskite structure[29] are 2.2 eV, 2.31–2.63 eV and 2.7 eV, respectively. So theoretically it can absorb visible light up to 560 nm, allowing about 25% of the solar energy to be absorbed. The optical absorption spectrum can also be adjusted by manipulating the ferroelectric material compositions through chemical doping or alloying. For example, in the $LiNbO_3$ or $KNbO_3$ crystals, Fe-doping extends the absorption edge to the region of 400–500 nm, corresponding to the excitation of electrons from Fe^{2+} ions to the conduction band of the crystals.[81] In $BaTiO_3$, Fe-doping can extend the absorption edge to around 647 nm.[82] Recently, ferroelectric bismuth titanate $Bi_4Ti_3O_{12}$ (BiT) with a wide bandgap tenability of 1 eV has been demonstrated by alloying it with Mott insulator $LaCoO_3$ (LCO). A unique unit cell structure, featured by an alternating arrangement of the BiT and LCO layers, has been demonstrated to systematically tune the optical bandgap of BiT from ~3.6 eV to ~2.7 eV with its strong ferroelectric property uninfluenced.[83] In addition, one general type of defects in ferroelectric oxide is the oxygen vacancy which can broaden the absorption spectrum if there is a large density. For example, the oxygen vacancies in the BFO film can extend the absorption spectrum to 560–650 nm.[77] The density of the oxygen vacancies can be controlled by thermal annealing, while the spatial distribution of the oxygen vacancies can be shifted by electrical pulses.[62,84–86] Interestingly, the light absorption was also reported to be enhanced by utilizing the internal photoelectric effect at the metal electrode, where the electrons excited from the metal electrode to the PZT film require photons with energy less than the bandgap of PZT. This component was also found to contribute to the measured photocurrent.[60]

In addition to the large optical bandgap, the small absorption coefficient of the ferroelectric materials is another issue limiting the photocurrent. A strong absorption allows a thinner film to be used which is beneficial for charge collection. Most oxides have very low absorption coefficients in the visible range. The absorption coefficient of PZT and BFO families (10^4 to 10^5 cm^{-1} at around 400 nm) is about three to four magnitudes higher than that of $LiNbO_3$ and $BaTiO_3$ materials (10–100 cm^{-1} at around 400 nm),[80,84,87,88] which enables a high light absorption in PZT and BFO films with a thickness of hundreds of nanometers. The optimized sample thickness for a maximized photocurrent is a tradeoff between light absorption and charge collection.

2.2.2 Exciton dissociation efficiency. The electron–hole pairs (or excitons) generated by incident photons with energy above the bandgap need to be dissociated efficiently to generate photocurrent. The binding energy of the excitons is inversely proportional to the dielectric constant of an active material. Fortunately, the dielectric constant of most ferroelectric materials (10^2 to 10^3) is much larger than that of organic and inorganic semiconductors (3–13), hence a small binding energy between holes and electrons is expected. According to the Glass model, the separation of the electrons and holes is driven by the noncentrosymmetric potential well in the unit cells.[11,22] The excited electrons generally shift along the polarization direction by only several angstroms before they decay, explaining the very small photocurrent in FE-PV devices.[33] From this point of view, it is necessary to increase the noncentrosymmetry of the crystal by developing new ferroelectric materials for improved photocurrents.[24,59,89,90] It is known that changing the chemical composition of ferroelectric materials can significantly change their crystal structures and thus the degree of noncentrosymmetry, which can affect the photovoltaic response.[91–93] For example, in the PZT ceramics, when the Zr/Ti atomic ratio varies from 48/53 to 54/46, the crystal structure changes from tetragonal to rhombohedral, where the latter shows stronger crystallographic asymmetry. Therefore in the lanthanum-doped PZT (PLZT) ceramics, the photocurrent was observed to increase by six times when the dopant loading was reduced from 6% to 4%.[91]

2.2.3 Charge collection efficiency. The next step after exciton dissociation is the collection of free charges. The charge collection efficiency is determined by the carrier lifetime, the carrier mobility and the electric field. The lifetime of the photogenerated nonthermalized charges in ferroelectric materials was thought to be in the picosecond scale,[17] while the recombination lifetime was measured to be sub-microseconds to tens of microseconds.[58,94] Reducing the thickness of the low conductive ferroelectric film can lead to increased charge collection efficiencies, *e.g.* Ichiki *et al.* compared the photovoltaic effects of the PLZT bulk crystal (with a thickness of 2.4 mm) and PLZT thin film (with a thickness of 4 μm) and found an improvement of over 100 times in the photocurrent.[28] However, the photovoltage was observed to decrease simultaneously when the thickness was reduced. Another apparent method to increase the charge collection efficiency is to increase the collecting electric field. For example, in the BFO based device, Zang *et al.* replaced the ITO electrode with nitric acid (HNO_3) treated graphene and observed a much increased photocurrent of 2.8 mA cm^{-2}, which was attributed

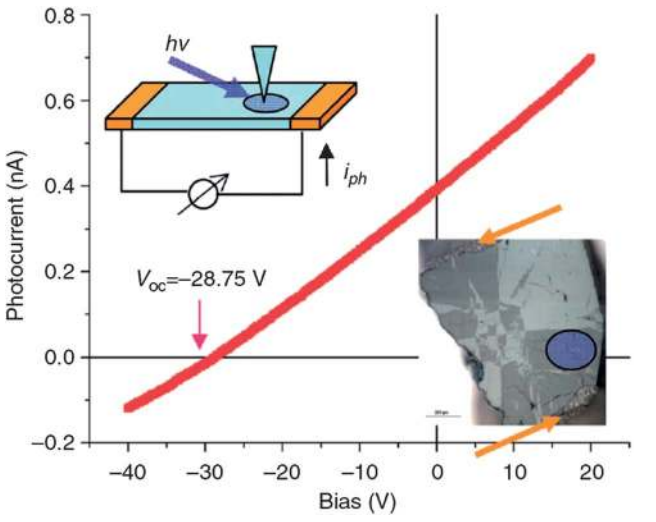

Fig. 4 Ultra-high efficient charge collection on the BFO crystal achieved by a conducting AFM tip demonstrated by Alexe *et al.*,[38] where the upper left image is the measurement setup, the lower inset shows the locations of the silver (Ag) electrode (yellow arrows) and the illuminated area on the BFO crystal.

to the extended depletion region throughout the entire ferroelectric layer by the formation of metal–intrinsic semiconductor–metal (MIM) structure.[78] It should be noticed that recently Alexe *et al.* observed a tip-enhanced photovoltaic effect in the BFO film, where the photogenerated carriers in the bulk of the BFO film were collected very efficiently by the AFM tips (Fig. 4).[38] The nonuniform local electric field due to a particular geometry of the tip contributed to the very high photocurrent density of 10–100 A cm^{-2} which is eight orders of magnitude higher than that in devices with parallel electrodes. This result might enable promising large-area ferroelectric photovoltaic devices with much improved photocurrent by using nano-tip arrays as the electrodes.

There has been an interesting idea on utilization of the increased depolarization field for enhanced charge collection efficiency. Since the depolarizing field is strongly influenced by the screening condition at the ferroelectric/electrode interface and film thickness,[46,68–71] an increased exciton dissociation as well as charge collection is expected by reducing the screening of the spontaneous polarization and the film thickness. Qin *et al.* did a theoretical calculation which suggested that the photocurrent in PLZT could be increased by tens of times by (1) replacing the metal electrode with semiconductors (reduced screening effect) and (2) reducing the PLZT thickness.[35] The maximum internal power conversion efficiency was calculated to be as high as 18.7% for an 8 nm thick PLZT film. However, when an ultra-thin FE layer is used, one accompanying problem is that the light absorption will be severely reduced. In the experimental part, Chen *et al.* studied the anomalous photovoltaic effect in the device with a structure of Au/polycrystalline BFO/Au and found that the photocurrent output was increased 24 times when the Au electrode was replaced by ITO, which was attributed to the increased depolarizing field.[72]

Table 1 Summary of the performance of the reported ferroelectric photovoltaic devices[a]

	Photovoltage		Photocurrent					
Device structure	V_{oc} (V)	L (μm)	I_{sc} (μA cm^{-2})	Light intensity (mW cm^{-2})	Light wavelength (nm)	Efficiency (P_{out}/P_{in}) (%)	Dominating working mechanism	FE-film fabrication methods
Pt/PZT(52/48)/Pt or Ni[102]	~0.8	0.2	~0.03	0.05	300–390	—	SC	Sol–gel
Pt/PLZT(3/52/48)/ITO[28]	0.86 ~496	4 2400	1700 ~16.8	150	—	—	BPV	MOD
Au/PLWZT(3/52/48)/Au[65]	7.0	25	—	1.11	365	—	BPV	Solution coating
Au/PLWZT(3/52/48)/Au[61]	0.6	0.706	—	0.74	365	—	SC	Sol–gel
Nb : $SrTiO_3$/PLZT (3/52/48)/LSM[35]	~0.7	0.068	~0.8	0.059	—	0.28	DF	Sputtering, epitaxial
Pt/PZT(20/80)/Pt[66]	—	0.36	~8	10	350–450	—	SC & BPV	Sputtering
$SrRuO_3$/BFO/ITO[36]	0.8–0.9	0.2	1500	285	Sunlight	10 (EQE)	SC	MOCVD
Au/BFO/Au[29]	~0.08	80	8.219	<20	532	—	SC	Mix-flux technique
$SrRuO_3$/BFO/Au[37]	0.286	0.17	0.4	750	435	—	SC	Sputtering, epitaxial
Pt/BFO/Pt[30]	16	200	120	285	W-light	10^{-3} (IQE)	DW	MOCVD
Pt/BFO/Pt[57]	0.014	One DW	50	100	W-light	10 (IQE)	DW	MOCVD
Pt : Pd/BFO/Pt : Pd[38]	6–30	50–300	10^7–10^8	40 000	405	40 (IQE)	TE & BPV	Mix-flux technique
Pt/Poly-BFO/Au and ITO[72]	0.1	0.3	~1	450	340	—	SC & DF	Sol–gel
Graphene/Poly-BFO/Pt[78]	0.20	0.3	2800	100	Sunlight	—	MIM–SC	Sol–gel
ZnO : Al/BFO/LSC[54]	0.22	0.35	~5	1	W-light	—	—	PLD
Au/BFO/Au[62]	~0.7	60	1.58	20	532	1.5 (EQE)	SC	Mix-flux technique
Nb-doped $SrTiO_3$/BFO/Au[79]	~0.15	0.1	6000	285	W-light	0.03	SC	PLD
Pt/Bi2FECrO6/Nb–$SrTiO_3$[32]	0.74	0.125	990	1.5	635	6.5	BPV	PLD, epitaxial
ITO/PZT/Cu_2O/Pt[39]	0.6	270	4800	100	Sunlight	0.57	SC	Sol–gel
ITO/PZT(53/47)/ITO[73]	0.45	0.4	0.006	0.45	—	0.6	SC & BPV	PLD
Ag/Pr-doped BFO NTs/Ag[89]	0.21	—	—	10	Sunlight	~0.5	—	Chemical template
Mg/PLZT(3/53/48)/ITO[60]	8.34	300	3.25	100	Sunlight	—	PE & BPV	HPC
FTO/Poly-BFO/AZO[74]	0.63	—	130	100	Sunlight	7 (EQE)	BI & DF	CSD
Fe/BFO/LSM/$SrTiO_3$[100]	0.21	—	48	20	W-light	—	SC & BPV	PLD, epitaxial

[a] PZT(a/b) = $PbZr_{a\%}Ti_{b\%}O_3$; PLZT($a/b/c$) = $Pb_{1-a\%}La_{a\%}Zr_{b\%}Ti_{c\%}O_3$; LSM = $LaSrMnO_3$; LSC = $LaSrCoO_3$; IQE = internal quantum efficiency; EQE = external quantum efficiency; DF = depolarization field effect; BPV = bulk photovoltaic effect; DW = domain wall effect; SC = Schottky contact effect; MIM = metal/insulate/metal junction, PE = photoelectric effect; BI = built-in potential due to asymmetric electrodes; TE = tip enhancement effect; MOD = metal–organic decomposition; MOVCD = metal–organic vapor phase epitaxial; PLD = pulsed laser deposition; HPC = hot-pressing calcinations; CSD = chemical solution deposition.

2.3 Other characteristics of FE-PV devices

Another unique property of the FE-PV devices is that their photovoltaic output is switchable with the polarization. Generally, the photovoltages in the opposite poling direction should be symmetric, *i.e.* $|V_{+\text{poling}}| = |V_{-\text{poling}}|$, but the symmetry can be lost due to other effects such as an additional built-in electric field coming from the work function difference of the electrodes and graded composition in FE films.[36,37,61,62,66] On the other hand, the magnitude of the photovoltage after multiple switching tends to systematically decrease due to ferroelectric fatigue. The ferroelectric fatigue is a common behavior in ferroelectric materials which can result from (1) charge trapping at the domain wall or near the electrode which screens the polarization field;[61,95–98] (2) the formation of defects, such as oxygen vacancies, at the FE/electrode interface which pins the domain boundaries and hinders their movements under an applied electric field;[98] (3) the formation of cracks or de-adhesion of the film from the substrate from due to the residual tensile or compressive stress.[99] Recently, Guo *et al.* demonstrated a novel non-volatile memory array based on the photovoltaic effect in BFO, where the photovoltaic output (V_{oc} or J_{sc}) was used as the read-out signal. The photovoltage output can be robustly switched between 0.11 V and −0.23 V for up to 10^8 cycles.[100]

In ferroelectric materials, the rising time of the photocurrent was reported to be about 10^{-5} s.[58] The response speed of the photovoltage is pretty slow. The saturation of the photovoltage output under a continuous illumination takes tens to hundreds of seconds,[94] which is several orders of magnitude slower than that in the conventional PV effect. The slow response time is thought to be related to the very small photoconductivity.[81,101] In general, larger photocurrents lead to faster photovoltaic response. Hence it is not surprising that the response time is also dependent on the light intensity and wavelength.[102]

To date, numerous inorganic FE-PV devices have been studied. The device structures, photovoltaic performance and the dominating working mechanisms of the related devices are summarised in Table 1.

3. Recent progress in the integration of ferroelectric materials in organic photovoltaic devices

Although there is no demonstration of efficient photovoltaic devices based on the FE-PV effect yet, there has been significant progress recently in the integration of ferroelectric materials in traditional p–n junction photovoltaic devices to overcome the challenges in these traditional devices. Here the working principles and challenges in organic photovoltaic devices are introduced and approaches to address them are reviewed.

3.1 Introduction to organic solar cells and the challenge in efficiency enhancement

A typical OPV device consists of one or more layers of organic materials located between a transparent electrode coated on substrates like glass or flexible polymer substrates and a metal cathode of Al, as shown in Fig. 5a. The organic layer is generally as thin as 80–200 nm because of the large absorption coefficient (10^5 cm^{-1}) and relatively low carrier mobility (10^{-4} to 10^{-1} cm^2 V^{-1} s^{-1}) of many organic molecules. Due to the high binding energy (0.4–1.0 eV) of Frenkel-excitons in organic semiconductors, photo-generated excitons cannot be dissociated by the weak built-in electric field provided by the electrode work function difference.[103] A donor–acceptor type heterojunction is generally formed in OPVs to dissociate excitons.[104,105] The photoactive layer can be either a blend or a layered structure. Studies of OPVs reveal that the light to electricity conversion involves four steps, which are labeled in Fig. 5b: (1) light absorption to generate an exciton; (2) exciton diffusion; (3) charge transfer between the donor and acceptor (after this step the electrons and holes locate in different materials, but are still electrically bound together due to the low dielectric constant of organic material and proximity between them – these are referred to as charge transfer excitons (CTEs),[106–110] to distinguish them from Frenkel-excitons); and (4) separation of the CTEs into free charges and extraction of the free charges to electrodes.[111]

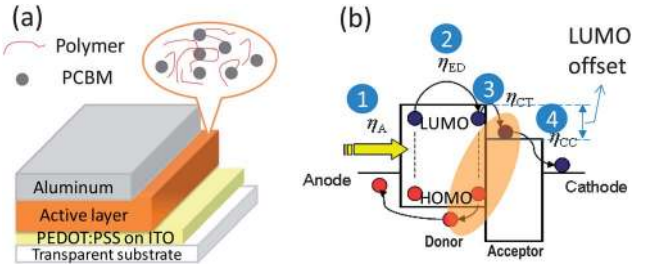

Fig. 5 (a) The device structure of a typical BHJ-OPV; (b) process of the conversion of incident light into electricity in OPVs. The electrons on the acceptor are still bound to holes on the donor right after the charge transfer, as illustrated by the ellipse in the figure.

The inefficient charge extraction issue remains a grand challenge for bulk-heterojunction (BHJ)-OPVs. The inefficient charge extraction is caused by the low carrier mobility of the existing polymer semiconductors,[112] which yields strong recombination of both bound electron–hole pairs and free charges. As illustrated in Fig. 5, the recombination of electron–hole pairs occurs in multiple paths: (1) Frenkel-exciton recombination before the photo-induced electron transfer, (2) CTE recombination (or geminate recombination) of the bound electron–hole pair after the photo-induced electron transfer, (3) Schottky–Read–Hall (SRH) recombination at the interfacial traps, dead-ends, and in the disordered band-tails, and (4) bimolecular recombination of the free charges. The charge recombination mechanism in OPVs varies from material systems, material morphology, electric field, *etc.* In optimized BHJ devices, the Frenkel-exciton recombination and SRH recombination constitute only a small portion of the total recombination loss because the photo-induced electron transfer efficiency was shown to be almost 100% efficient.[113] The major charge recombination in most optimized OPVs falls into

two categories:[112,114] geminate recombination[113,115–118] and bimolecular recombination,[117,119–123] although the dominating charge recombination mechanism is presently under intense debate.[106,109,112,124]

Another grand challenge of OPV device efficiency enhancement is the significant energy loss during the charge transfer from the donor to the acceptor.[41] It is generally accepted that the LUMO level offset between the donor and acceptor should be larger than the exciton binding energy (0.3–0.5 eV) in order to get an efficient charge transfer. However, a smaller LUMO offset of 0.12 eV has been reported recently which could also result in efficient charge transfer.[125] Until now, most high efficiency polymer:fullerene-derivative systems have a very large LUMO offset around 1 eV between the donor and acceptor, which results in significant energy loss.

The existing bottlenecks of the FE-PV and organic solar cell devices indicate that the modification on either type of devices to enhance the device performance is shown to be inefficient. To tackle this issue, an effective way is to integrate the functionality of two types of materials into one cell to take advantage of their complementary properties. The ferroelectric materials can generate a huge permanent electric field, which is essential to assist the separation of electron–hole pairs and extraction of free charge carriers in the organic solar cells. Organic semiconductors have very strong absorption in the visible and near infrared range. The ferroelectric materials can be used as the interfacial layer between the active layers and electrodes,[40] between the donor and acceptor layers,[41] or be blended in the bulk films, which will be discussed in detail in the following part of this review.

3.2 Increasing the efficiency of organic photovoltaic devices by a ferroelectric polymer

3.2.1 Ferroelectric polymer polyvinylidene fluoride and its copolymer with trifluoroethylene. Polyvinylidene fluoride (PVDF) and its copolymers with TrFE, P(VDF–TrFE), are widely used room temperature ferroelectric materials because of their large polarization charge density and low fabrication cost. There is a large dipole moment of 6.4×10^{-30} C m pointing from fluorine to hydrogen atoms,[126] and the spontaneous polarization reaches 0.1 C m^{-2} for some co-polymers after the dipoles are aligned. The PVDF polymers usually have mixed crystalline and amorphous phases. It has been reported that pure PVDF only has a degree of crystallinity of 50%, while P(VDF–TrFE) can reach almost 100% crystallinity.[127] There are four phases for the P(VDF–TrFE) copolymer, *i.e.* the paraelectric α phase, ferroelectric β, δ and γ phases.[128] More details of the organic ferroelectronics and P(VDF–TrFE) can be found in other references.[126,129]

Ferroelectric polymers, such as P(VDF–TrFE), can be deposited by various methods including spin coating,[130] electrospinning,[131] nano-imprinting,[40,132,133] and Langmuir–Blodgett (LB) deposition.[70,75] The spin coating from a low boiling point solvent usually leads to an amorphous film, which can be thermally annealed to increase its ferroelectric phase at a temperature higher than its Curie point. The LB method has been used to deposit high quality P(VDF–TrFE) monolayers.[134]

A similar bulk photovoltaic effect has been observed in polymer films based on PVDF and its derivatives, where a V_{oc} of ~50 V and a power conversion efficiency of ~0.25% under UV illumination has been reported.[135] The polymer FE-PV devices possess good flexibility as compared to those in-organic FE-PV devices.

3.2.2 Ferroelectric P(VDF–TrFE) layer at the semiconductor/electrode interface to induce an electric field. As introduced above, the internal electric field generated by the work function difference between two electrodes is insufficient so that not all of the electron–hole pairs can be dissociated under short-circuit conditions in many polymer material systems. Although the charge recombination processes in BHJ OPVs are complicated, a straightforward approach to enhance the charge collection efficiency is to apply a large electric field (or reverse bias), which is evident in the application of the photodetectors. However it is not feasible to apply an external electric field in a solar cell device.

To tackle this issue, Yuan *et al.* incorporated a thin layer of ferroelectric P(VDF–TrFE) at the organic/electrode interface to generate an extra electric field in the active layer. The ferroelectric layer was deposited on poly(3-hexylthiophene):phenyl-C_{61}-butyric acid methyl ester (P3HT:PCBM) surface by the LB method, followed by a thermal annealing process to convert it into the ferroelectric phase.[40] After poling under negative bias, the dipoles in the FE layer are aligned with their positive polarization charges close to the P3HT:PCBM layer and the negative polarization charges close to the Al layer, as illustrated in Fig. 6a. The negative polarization charges are neutralized by the electrode due to the large density of free charges in metal.

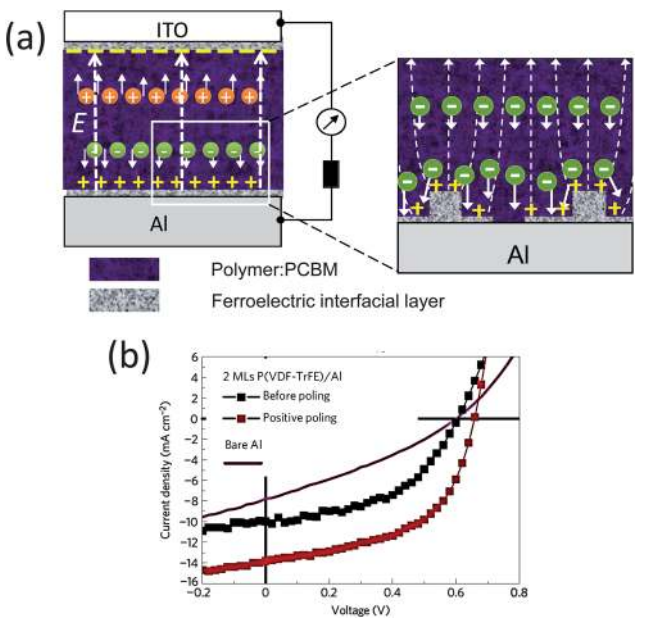

Fig. 6 (a) Schematics of FE-OPV and working principle with the ferroelectric polymer at the interface; (b) photocurrent curves of a poly(4,4-dioctyldithieno(3,2-*b*:2′,3′-*d*)silole)-2,6-diyl-*alt*-(2,1,3-benzothiadiazole)-4,7-diyl (PSBTBT):phenyl-C71-butyric-acid-methyl ester (PC70BM) device without an FE layer (magenta line), with an FE layer before poling (black square line) and after poling (red squares).[40]

The positive polarization charges can generate an electric field penetrating through the organic active layer. This additional electric field can facilitate the dissociation of the bound electron–hole pairs and charge collection, leading to increased J_{sc}, FF and V_{oc}. The typical photocurrents of the devices before and after poling are shown in Fig. 7b. The PCEs of poled FE-OPV devices were about twice larger compared to the devices without FE layers for many types of polymer systems tested. The efficiencies of these devices are higher than the optimized ones with other methods. From the enhanced photocurrent in the FE-OPV devices, the additional electric field induced by the ferroelectric layers was estimated to be about 12 V μm^{-1}, which is much larger than the built-in electric field ($\sim$4 V μm^{-1}) caused by the work function difference between the anode and cathode. The induced electric field was actually limited by the incomplete coverage of the P(VDF–TrFE) on the P3HT:PCBM surface. There is still much space for the improvement because the electric field induced by 3 monolayers of P(VDF–TrFE) was calculated to be as large as 50 V μm^{-1}.

One issue in applying this method to the recently developed low bandgap polymer for efficiency enhancement is that the LB deposition used to fabricate monolayers of P(VDF–TrFE) films is not compatible with the process of these polymers due to the high temperature thermal annealing around 130 °C needed to convert the P(VDF–TrFE) LB film into the ferroelectric phase. For example, many state-of-the-art low bandgap polymers, such as poly[*N*-9′-hepta-decanyl-2,7-carbazole-*alt*-5,5-(4′,7′-di-2-thienyl-2′,1′,3′-enzothiadiazole)] (PCDTBT), poly[4,8-bis-(2-ethyl-hexyl-thiophene-5-yl)-benzo[1,2-*b*:4,5-*b*′]dithiophene-2,6-diyl]-*alt*-[2-(2′-ethyl-hexanoyl)-thieno[3,4-b]thiophen-4,6-diyl (PBDTTT-C-T)] and poly[thieno[3,4-*b*]thiophene/benzodithiophene] (PTB7), cannot be thermally annealed at temperatures above 70 °C which otherwise results in the formation of oversized polymers or/and PCBM domains. This thermal treatment can be avoided if ferroelectric P(VDF–TrFE) can be directly deposited on the polymer:PCBM surface. For this purpose, a simple solvent chemistry method for the synthesis of ferroelectric phase P(VDF–TrFE) nano-crystals was developed by Xiao *et al.*[130] The amorphous P(VDF–TrFE) nanoparticles with a diameter of 60–100 nm were firstly synthesized using acetone as a good solvent and methanol : water blend as a bad solvent. The hydrophobic interaction between water and fluorine atoms in P(VDF–TrFE) leads to the aggregation of P(VDF–TrFE) chains and formation of amorphous ball like NPs. The size of the NPs can be controlled by tuning the volume blend ratio of methanol : water from 300–500 nm (1 : 0 v/v) to 60–100 nm (10 : 1 v/v). Then the amorphous P(VDF–TrFE) NPs were converted into the ferroelectric phase by refluxing them in liquid. The preformed ferroelectric nano-crystals enable the fabrication of FE-OPV devices without annealing the PCDTBT:PC_{70}BM layer, resulting in a high efficiency of 6.7% which is 20% higher than that of the optimized device using low work function metal calcium as the electrode.

This approach has been shown to be universal and is followed by several other groups. It has been shown that the ferroelectric layer is not necessarily located at the cathode electrode side. For example, by inserting the P(VDF–TrFE) into the interface between the PEDOT:PSS layer and organic active layer, Rastogi also obtained an improved photocurrent from $\sim$5.2 mA cm^{-2} to $\sim$9 mA cm^{-2}.[136] It was observed that the photocurrent systematically increased with the magnitude of the poling voltages, demonstrating the key role of the electric field introduced by the aligned ferroelectric layer which facilities the charge extraction.[136]

It was also proposed that ferroelectric materials such as $BaTiO_3$ or PZT can be used at the front/rare surface of inorganic photovoltaic devices, wherein the surface charge caused by the polarized ferroelectric materials can induce an electric field inside the semiconductor layer to prevent the electron–hole recombination occurring around the front/rare surface.[137] An increased power conversion efficiency and V_{oc} was hence expected. Similarly, the ferroelectric polymer P(VDF–TrFE) was also suggested to be used in inorganic photovoltaics. The surface charge at the interface between P(VDF–TrFE) and the inorganic semiconductor could lead to the formation of an inversion layer which helps to separate the electron–hole pairs.[138]

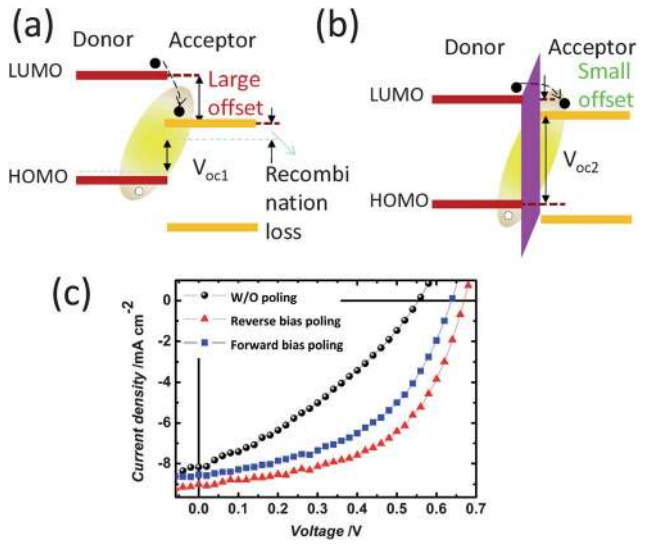

Fig. 7 The energy level diagram of the semiconductor hetero-structure without (a) and with (b) a dipole layer inserted at the D/A interface. (c) Photocurrent curves for the as-made device (black balls), after poling the P(VDF–TrFE) layer with reverse bias (red triangles) and forward bias pulses (blue squares).[41]

3.2.3 Ferroelectric P(VDF–TrFE) layer at the p/n interface to shift the relative energy levels. Another attracting application of incorporating the P(VDF–TrFE) in OPV devices for efficiency enhancement is to tune the relative energy level of donor and acceptor for maximizing the V_{oc} output.[41] The concept is illustrated in Fig. 7a and b. A smaller energy offset of the donor and acceptor is highly desired to reduce the energy loss during the charge transfer process. This concept can be realized by designing new materials with substituted functional groups.[139,140] For example, Zhong *et al.* synthesized fluoroalkylated P3HT and PCBM to shift the energy level of the donor and acceptor and applied them in a bilayer device. The fluoroalkyl groups on P3HT or/and PCBM spontaneously form a surface-segregated monolayer on the spin coated film due to their low surface energy, which induced aligned

dipoles at the D/A interface.[140] Alternatively, tuning the D/A energy offset with aligned ferroelectric dipoles can avoid changing the polymer chemical structures. Many polymers show promising properties in many other aspects, such as bandgap, absorption coefficient, solubility, and charge mobilities, but a too large LUMO offset. Therefore, using a ferroelectric interfacial layer is a general approach applicable to all polymer systems and it should have minimal influence on other properties of the semiconducting polymers. Yang *et al.* demonstrated an increased V_{oc} in the P3HT/PCBM bilayer device by inserting a monolayer of P(VDF–TrFE) LB film between P3HT and PCBM.[41] The energy level shift, ΔE, caused by the dipole layer can be estimated by: $\Delta E = d\sigma_P q/\varepsilon_0\varepsilon_{FE}$, where d is the thickness of the ferroelectric layer, σ_P is the polarization charge density, q is the elemental charge, ε_0 and ε_{FE} are the dielectric constant of the vacuum and relative dielectric constant ferroelectric layer, respectively. Theoretically, an 0.6 nm thick P(VDF–TrFE) layer between the donor and acceptor can lead to an energy level shift by 0.8 eV which is enough for all these applications. Interestingly, the insertion of the ferroelectric dipole layer between the donor and acceptor layer did not inhibit the charge transfer from the donor to the acceptor. A strong charge transfer was found after aligning the ferroelectric dipoles in a preferred direction, which was evidenced by the stronger photoluminescence quench in the D/FE/A trilayer film than in the D/A bilayer film. According to the Marcus theory, it has been observed that the charge transfer rate can be significantly altered by changing the LUMO offset because of the changed electron cloud coupling between the donor and acceptor.[141] Using a ferroelectric interfacial layer hence provides an effective approach for the optimization of the charge transfer rate. As shown in Fig. 7c, the V_{oc} was increased from 0.55 V to 0.67 V after aligning the dipoles of the ferroelectric layer with a negative external bias, exceeding all other observed V_{oc} values in either bulk or bilayer devices for the P3HT:PCBM system. However, the coverage of the P(VDF–TrFE) layer on the P3HT surface deposited by the LB method was only around 20%, which causes a large portion of P3HT to directly contact with PCBM materials, thus limiting a potential increase in V_{oc}. For this concern, great effort is being made to increase the coverage of the ferroelectric layer by better controlling the ferroelectric layer processing technique. Furthermore, the morphology and uniformity of ferroelectric film also need to be improved for better device performance. A prospect of this work is that the V_{oc} can be enhanced to about 1.0–1.5 V if 100% coverage of ferroelectric film is achieved.

3.2.4 Mixing P(VDF–TrFE) into bulk heterojunction films. Mixing the photoactive materials with the ferroelectric materials is another approach to utilize the large local electric field of ferroelectric molecules for efficiency enhancement in OPV devices. By mixing a small amount of P(VDF–TrFE) polymer into the bulk P3HT:PCBM films, Nalwa *et al.* enhanced the charge collection efficiency and achieved a very high internal quantum efficiency of 100%.[142] According to a classic dipole-electric field model: $E = 4\pi\sigma f/\varepsilon_0\varepsilon_{FE}$, where σ is the surface charge density and f is the volume fraction of the dipoles, the electric field generated by the P(VDF–TrFE) was estimated to be as large as 240 V μm^{-1} when the volume fraction of P(VDF–TrFE) was 3%. The local electric field induced by the ferroelectric dipoles is much larger than the electric field needed to dissociate CTEs which is around 50–70 V μm^{-1}. The higher exciton dissociation rate in the device with the blended ferroelectric polymer was supported by a shorter photoluminescence lifetime in the P(VDF–TrFE) mixed P3HT:PCBM film (73 ps) than that in the controlled film without the ferroelectric polymer (100 ps), implying an increased exciton dissociation rate caused by the local electrical field.

3.3 Switchable property of FE-OPV devices

One unique property of inorganic FE-PV and FE-OPV devices is their switchable photocurrents and dark currents controlled by the polarization direction of the ferroelectric layer. For the FE-OPV device with P(VDF–TrFE) at the organic/electrode interface, the generated electric field is expected to be switched parallel or antiparallel with the built-in field, resulting in better and worse device performance.[40,130,136] This was clearly demonstrated by Yuan *et al.* as shown in Fig. 8a. By inserting the P(VDF–TrFE) at both anode and cathode sides as interfacial layers, the diode polarity of the OPV device based on P3HT:PCBM was switched under different poling directions, as shown in Fig. 8b.[40,132] This is the first time both the switchable diode and photovoltaic effect was demonstrated in FE-PV devices. For the device with P(VDF–TrFE) mixed in the P3HT:PCBM bulk film, the J_{sc}, V_{oc} and FF also showed switchable variation under different poling directions.[142] For the device with P(VDF–TrFE) inserted at the donor and acceptor interface, the LUMO offset between the donor and acceptor can be tuned as well by the different dipole directions of the ferroelectric layer, which results in a switchable V_{oc} between 0.55 V and 0.67 V.[41]

It should be noted that only the ferroelectric phase of P(VDF–TrFE) has aligned dipoles after external applied bias. The amorphous P(VDF–TrFE) film, *e.g.* formed by spin coating from a low boiling point solvent, only works as a dielectric layer, so that OPV devices with P(VDF–TrFE) spin-coated from acetone did not show switchable performance.[132,143]

3.4 Stability of the polarization of a ferroelectric layer in FE-OPV devices

In order to apply the FE-PV or FE-OPV devices for solar energy harvesting, the polarization of the ferroelectric polymer should be very stable both in the dark and under illumination. It is still under debate about the polarization stability of the ferroelectric material at the metal/semiconductor interface. Naber *et al.* claimed that the polarization of P(VDF–TrFE) in the metal/P(VDF–TrFE)/semiconductor (P3HT) (MIS) structure was not stable due to a lack of minority electrons to compensate the spontaneous polarization charges.[144] However, many other results showed that the polarization of a ferroelectric material can be stable on a semiconductor and even on an insulator. Kalbitz *et al.* showed that the polarization of P(VDF–TrFE) in the MIS structure was very stable at either direction, demonstrated by the full ferroelectric polarization hysteretic loop. The trapped electrons at the interface between the poled P(VDF–TrFE) crystallites and the p-type semiconductor were sufficient to compensate the spontaneous polarization charges.[145] In the case of P(VDF–TrFE) inserted between a metal electrode and

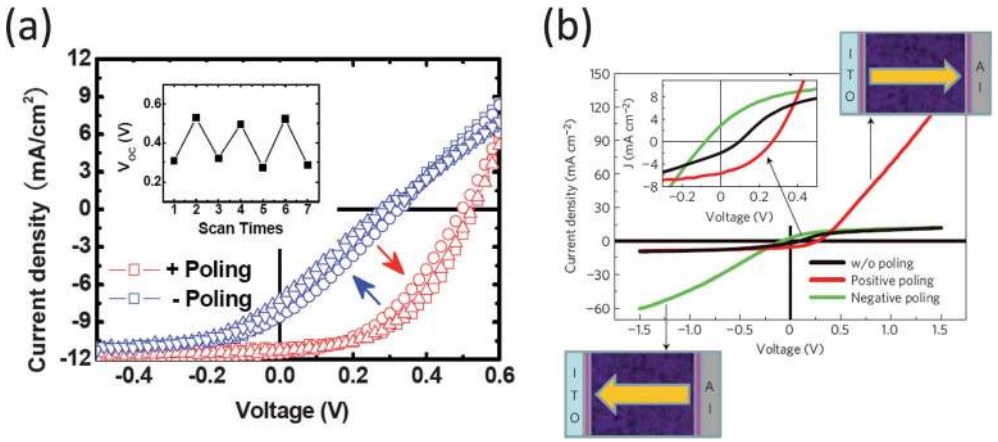

Fig. 8 Switching property of the P3HT:PCBM device. (a) Device with P(VDF–TrFE) at the cathode interface, (b) device with P(VDF–TrFE) at both cathode and anode interfaces.[40]

insulator, Horie *et al.* also observed a full ferroelectric polarization hysteretic loop for the device with a structure of metal/VDF/aluminium oxide (Al_2O_3)/Al. The polarization could be repeated more than 10 000 times.[146]

The polarization of the ferroelectric polymer was shown to be very stable even without a top electrode. For example, Hu *et al.* used the nano-imprinting process to fabricate nano-arrays of P(VDF–TrFE) on top of high doped silicon substrates with a thickness of around 50 nm. A PFM tip was used to switch the dipoles. It was found that the polarization could be switched up or down. The polarization was found to be very stable after one day even without a top electrode.[133] Sharma *et al.* deposited an ultrathin ferroelectric P(VDF–TrFE) layer on a highly doped Si substrate using the LB method and used the PFM to measure its ferroelectric switching. A quite symmetric hysteresis loop with a symmetry coercive field was observed for the nanomesa of the P(VDF–TrFE) and the polarization was very stable without a top electrode.[147] Most strikingly, it was demonstrated that the epitaxial $BaTiO_3$ (with thickness varying from 1.6 nm to 40 nm) showed stable and switchable polarization on insulating silicon oxides without a top electrode.[148]

In the OPV devices with P(VDF–TrFE) inserted at the cathode interface, Yuan *et al.* reported that the polarization was very stable for more than two weeks, supported by the non-degraded performance of the device.[132] In the device with the P(VDF–TrFE) layer inserted at the anode side between the PEDOT:PSS and P3HT:PCBM layer, Rastogi *et al.* observed a full ferroelectric polarization hysteresis loop. By inserting the P(VDF–TrFE) layer between two semiconducting P3HT:PCBM layers, a full hysteresis loop was also observed, indicating that the polarization on both directions was stable.[136]

All the above reported results suggest that the polarization of the ferroelectric P(VDF–TrFE) layer with one semiconducting electrode in the SIM structure, or sandwiched between two organic semiconducting layers, or even with only one electrode is stable. One reason may be that the trapped charges at the P(VDF–TrFE)/semiconductor interface are sufficient to compensate the polarization charges of the ferroelectric layer.[145]

4. Summary and outlook for future development of FE-PV devices

The research into FE-PV devices is still increasing with contributions from better material engineering and new approaches to utilizing the ferroelectric dipoles. One major direction in pure FE-PV device development could be reduction of the bandgap of the ferroelectric materials and increase of the carrier lifetime so that more free charges can be generated by sunlight and extracted out of the devices. The electronic structures and the electrical properties of the semiconductor materials are highly sensitive to the unit cell structure and chemical substitution. A recent example is from the studies of the halide perovskite photovoltaic device, where the electron–hole diffusion length in solution-processed $CH_3NH_3PbI_3$ was found to be increased by about ten times when some of the iodine ions in the perovskite structure were replaced by chloride ions.[149,150] From this point of view, it is crucial to develop new ferroelectric materials or functional microscopic structures with the guidance of first-principles calculation. FE-PV devices based on ferroelectric nanomaterials such as nanowires or nanoparticles might be another possible direction, where the unit cell and its corresponding ferroelectric/piezoelectric properties are supposed to be significantly influenced by the surface effect.[134,151–155] Besides, the distribution of the depolarization field in the ferroelectric nanomaterials should be very different from that in thin film structures because of the different screening effect in nanostructured materials.[156–158] It is also believed that ferroelectric materials will find more applications in traditional p–n junction photovoltaic devices. The semiconductor materials used in traditional p–n junction photovoltaic devices have advantages in charge transport and light absorption. On the other hand, the polarization charges caused by the remnant polarization can play a role in the separation of the photogenerated charge carrier-pairs and the transportation of the carriers by introducing an extrinsic electrical field in the active layers; meanwhile the aligned dipoles in the ferroelectric materials provide a promising way to control the barrier height, interfacial energy

offset or the width of the depletion region, all of which mentioned above are crucial in the photovoltaic devices.

Acknowledgements

We thank the financial support by the National Science Foundation under Awards ECCS-1201384 and ECCS-1252623, and the Nebraska Public Power District through the Nebraska Center for Energy Sciences Research.

References

1 T. Tsoutsos, N. Frantzeskaki and V. Gekas, *Energy Policy*, 2005, **33**, 289–296.
2 A. Zahedi, *Renewable Energy*, 2006, **31**, 711–718.
3 M. A. Green, *Solar cells: operating principles, technology, and system applications*, Englewood Cliffs, NJ, Prentice-Hall, Inc., 1982.
4 P. Würfel and U. Würfel, *Physics of Solar Cells: From Basic Principles to Advanced Concepts*, http://wiley.com, 2009.
5 A. Shah, P. Torres, R. Tscharner, N. Wyrsch and H. Keppner, *Science*, 1999, **285**, 692–698.
6 D. E. Carlson and C. R. Wronski, *Appl. Phys. Lett.*, 1976, **28**, 671–673.
7 M. G. Panthani, V. Akhavan, B. Goodfellow, J. P. Schmidtke, L. Dunn, A. Dodabalapur, P. F. Barbara and B. A. Korgel, *J. Am. Chem. Soc.*, 2008, **130**, 16770–16777.
8 J. Burschka, N. Pellet, S.-J. Moon, R. Humphry-Baker, P. Gao, M. K. Nazeeruddin and M. Gratzel, *Nature*, 2013, **499**, 316–319.
9 J. Britt and C. Ferekides, *Appl. Phys. Lett.*, 1993, **62**, 2851–2853.
10 S. A. McDonald, G. Konstantatos, S. Zhang, P. W. Cyr, E. J. D. Klem, L. Levina and E. H. Sargent, *Nat. Mater.*, 2005, **4**, 138–142.
11 C. W. Tang, *Appl. Phys. Lett.*, 1986, **48**, 183–185.
12 M. M. Lee, J. Teuscher, T. Miyasaka, T. N. Murakami and H. J. Snaith, *Science*, 2012, **338**, 643–647.
13 A. Kojima, K. Teshima, Y. Shirai and T. Miyasaka, *J. Am. Chem. Soc.*, 2009, **131**, 6050–6051.
14 M. Liu, M. B. Johnston and H. J. Snaith, *Nature*, 2013, **501**, 395–398.
15 R. Von Baltz, *Phys. Status Solidi B*, 1978, **89**, 419–429.
16 A. G. Chynoweth, *Phys. Rev.*, 1956, **102**, 705–714.
17 V. Fridkin, *Crystallogr. Rep.*, 2001, **46**, 654–658.
18 L. Pintilie, I. Vrejoiu, G. Le Rhun and M. Alexe, *J. Appl. Phys.*, 2007, **101**, 064109.
19 L. Arizmendi, *Phys. Status Solidi A*, 2004, **201**, 253–283.
20 V. M. Fridkin and B. Popov, *Sov. Phys. Usp.*, 1978, **21**, 981–991.
21 A. Glass, D. Von der Linde and T. Negran, *Appl. Phys. Lett.*, 1974, **25**, 233–235.
22 A. Glass, D. Von der Linde, D. Auston and T. Negran, *J. Electron. Mater.*, 1975, **4**, 915–943.
23 J. Carnicero, O. Caballero, M. Carrascosa and J. Cabrera, *Appl. Phys. B*, 2004, **79**, 351–358.
24 B. Kang, B. K. Rhee, G.-T. Joo, S. Lee and K.-S. Lim, *Opt. Commun.*, 2006, **266**, 203–206.
25 P. S. Brody and F. Crowne, *J. Electron. Mater.*, 1975, **4**, 955–971.
26 M. Ichiki, Y. Morikawa and T. Nakada, *Jpn. J. Appl. Phys., Part 1*, 2002, **41**, 6993–6996.
27 M. Ichiki, Y. Morikawa, K. Nonaka, T. Nakada, C. Endo and R. Maeda, in *Photovoltaic effect of PLZT in a layered film structure and its application to ultraviolet sensing, Microprocesses and Nanotechnology Conference, 2003. Digest of Papers, 2003 International*, IEEE, 2003, pp. 184–185.
28 M. Ichiki, R. Maeda, Y. Morikawa, Y. Mabune, T. Nakada and K. Nonaka, *Appl. Phys. Lett.*, 2004, **84**, 395–397.
29 T. Choi, S. Lee, Y. J. Choi, V. Kiryukhin and S. W. Cheong, *Science*, 2009, **324**, 63–66.
30 S. Y. Yang, J. Seidel, S. J. Byrnes, P. Shafer, C. H. Yang, M. D. Rossell, P. Yu, Y. H. Chu, J. F. Scott and J. W. Ager, *Nat. Nanotechnol.*, 2010, **5**, 143–147.
31 W. Ji, K. Yao and Y. C. Liang, *Phys. Rev. B: Condens. Matter Mater. Phys.*, 2011, **84**, 094115.
32 R. Nechache, C. Harnagea, S. Licoccia, E. Traversa, A. Ruediger, A. Pignolet and F. Rosei, *Appl. Phys. Lett.*, 2011, **98**, 202902.
33 V. M. Fridkin, *Photoferroelectrics*, Springer, 1979.
34 B. I. S. K. Sturman and V. M. Fridkine, *The photovoltaic and photorefractive effects in noncentrosymmetric materials*, CRC Press, 1992.
35 M. Qin, K. Yao and Y. C. Liang, *Appl. Phys. Lett.*, 2008, **93**, 122904.
36 S. Yang, L. Martin, S. Byrnes, T. Conry, S. Basu, D. Paran, L. Reichertz, J. Ihlefeld, C. Adamo and A. Melville, *Appl. Phys. Lett.*, 2009, **95**, 062909.
37 W. Ji, K. Yao and Y. C. Liang, *Adv. Mater.*, 2010, **22**, 1763–1766.
38 M. Alexe and D. Hesse, *Nat. Commun.*, 2011, **2**, 256.
39 D. Cao, C. Wang, F. Zheng, W. Dong, L. Fang and M. Shen, *Nano Lett.*, 2012, **12**, 2803–2809.
40 Y. Yuan, T. J. Reece, P. Sharma, S. Poddar, S. Ducharme, A. Gruverman, Y. Yang and J. Huang, *Nat. Mater.*, 2011, **10**, 296–302.
41 B. Yang, Y. Yuan, P. Sharma, S. Poddar, R. Korlacki, S. Ducharme, A. Gruverman, R. Saraf and J. Huang, *Adv. Mater.*, 2012, **24**, 1455–1460.
42 C. Wang, D. Cao, F. Zheng, W. Dong, L. Fang, X. Su and M. Shen, *Chem. Commun.*, 2013, **49**, 3769–3771.
43 L. Li, G. S. Rohrer and P. A. Salvador, *J. Am. Ceram. Soc.*, 2012, **95**, 1414–1420.
44 L. Li, Y. Zhang, A. M. Schultz, X. Liu, P. A. Salvador and G. S. Rohrer, *Catal. Sci. Technol.*, 2012, **2**, 1945–1952.
45 D. Tiwari and S. Dunn, *J. Mater. Sci.*, 2009, **44**, 5063–5079.
46 M. Qin, K. Yao, Y. C. Liang and S. Shannigrahi, *J. Appl. Phys.*, 2007, **101**, 014104–014108.
47 P. Brody, *Solid State Commun.*, 1973, **12**, 673–676.
48 P. S. Brody, *Appl. Phys. Lett.*, 1981, **38**, 153–155.
49 M. Ichiki, H. Furue, T. Kobayashi, R. Maeda, Y. Morikawa, T. Nakada and K. Nonaka, *Appl. Phys. Lett.*, 2005, **87**, 222903.
50 M. Ichiki, Y. Morikawa, Y. Mabune and T. Nakada, *J. Eur. Ceram. Soc.*, 2004, **24**, 1709–1714.

51 P. Poosanaas, K. Tonooka and K. Uchino, *Mechatronics*, 2000, **10**, 467–487.
52 P. Brody and B. Rod, *Integr. Ferroelectr.*, 1993, **3**, 245–257.
53 A. Matsumura, Y. Kamaike, T. Horiuchi, M. Shimizu, T. Shiosaki and K. Matsushige, *Jpn. J. Appl. Phys., Part 1*, 1995, **34**, 5258–5262.
54 R. Katiyar, A. Kumar, G. Morell, J. Scott and R. Katiyar, *Appl. Phys. Lett.*, 2011, **99**, 092906.
55 Y. Yao, B. Zhang, L. Chen, Y. Yang, Z. Wang, H. N. Alshareef and X. X. Zhang, *J. Phys. D: Appl. Phys.*, 2013, **46**, 055304.
56 G. Chanussot and A. Glass, *Phys. Lett. A*, 1976, **59**, 405–407.
57 J. Seidel, D. Fu, S.-Y. Yang, E. Alarcón-Lladó, J. Wu, R. Ramesh and J. W. Ager III, *Phys. Rev. Lett.*, 2011, **107**, 126805.
58 M. Alexe, *Nano Lett.*, 2012, **12**, 2193–2198.
59 S. M. Young and A. M. Rappe, *Phys. Rev. Lett.*, 2012, **109**, 116601.
60 J. Zhang, X. Su, M. Shen, Z. Dai, L. Zhang, X. He, W. Cheng, M. Cao and G. Zou, *Sci. Rep.*, 2013, **3**, 2109.
61 M. Qin, K. Yao, Y. C. Liang and B. K. Gan, *Appl. Phys. Lett.*, 2007, **91**, 092904.
62 H. Yi, T. Choi, S. Choi, Y. Oh and S. W. Cheong, *Adv. Mater.*, 2011, **23**, 3403–3407.
63 P. Zhang, D. Cao, C. Wang, M. Shen, X. Su, L. Fang, W. Dong and F. Zheng, *Mater. Chem. Phys.*, 2012, **135**, 304–308.
64 B. K. Gan, K. Yao, S. C. Lai, Y. F. Chen and P. C. Goh, *IEEE Electron Device Lett.*, 2008, **29**, 1215–1217.
65 K. Yao, B. K. Gan, M. Chen and S. Shannigrahi, *Appl. Phys. Lett.*, 2005, **87**, 212906.
66 F. Zheng, J. Xu, L. Fang, M. Shen and X. Wu, *Appl. Phys. Lett.*, 2008, **93**, 172101.
67 C. Ahn, K. Rabe and J.-M. Triscone, *Science*, 2004, **303**, 488–491.
68 R. Mehta, B. Silverman and J. Jacobs, *J. Appl. Phys.*, 1973, **44**, 3379–3385.
69 I. Batra, P. Wurfel and B. Silverman, *Phys. Rev. B: Solid State*, 1973, **8**, 3257.
70 P. Wurfel and I. Batra, *Phys. Rev. B: Solid State*, 1973, **8**, 5126.
71 D. Kim, J. Jo, Y. Kim, Y. Chang, J. Lee, J.-G. Yoon, T. Song and T. Noh, *Phys. Rev. Lett.*, 2005, **95**, 237602.
72 B. Chen, M. Li, Y. Liu, Z. Zuo, F. Zhuge, Q.-F. Zhan and R.-W. Li, *Nanotechnology*, 2011, **22**, 195201.
73 B. Chen, Z. Zuo, Y. Liu, Q.-F. Zhan, Y. Xie, H. Yang, G. Dai, Z. Li, G. Xu and R.-W. Li, *Appl. Phys. Lett.*, 2012, **100**, 173903.
74 W. Dong, Y. Guo, B. Guo, H. Liu, H. Li and H. Liu, *Mater. Lett.*, 2012, **91**, 359–361.
75 W. Dong, Y. Guo, B. Guo, H. Li and H. Liu, *Mater. Lett.*, 2012, **88**, 140–142.
76 H. Sharma, S. Bobby Singh and N. Boinis Singh, *Phys. B*, 2011, **406**, 351–353.
77 W. M. Lee, J. H. Sung, K. Chu, X. Moya, D. Lee, C. J. Kim, N. D. Mathur, S. W. Cheong, C. H. Yang and M. H. Jo, *Adv. Mater.*, 2012, **24**, OP49–OP53.
78 Y. Zang, D. Xie, X. Wu, Y. Chen, Y. Lin, M. Li, H. Tian, X. Li, Z. Li and H. Zhu, *Appl. Phys. Lett.*, 2011, **99**, 132904.
79 T. Qu, Y. Zhao, D. Xie, J. Shi, Q. Chen and T. Ren, *Appl. Phys. Lett.*, 2011, **98**, 173507.
80 S. Basu, L. Martin, Y. Chu, M. Gajek, R. Ramesh, R. Rai, X. Xu and J. Musfeldt, *Appl. Phys. Lett.*, 2008, **92**, 091905.
81 F. Lüdtke, N. Waasem, K. Buse and B. Sturman, *Appl. Phys. B*, 2011, **105**, 35–50.
82 G. Chanussot, V. Fridkin, G. Godefroy and B. Jannot, *Appl. Phys. Lett.*, 1977, **31**, 3–5.
83 W. S. Choi, M. F. Chisholm, D. J. Singh, T. Choi, G. E. Jellison Jr and H. N. Lee, *Nat. Commun.*, 2012, **3**, 689.
84 A. Dhar and A. Mansingh, *J. Appl. Phys.*, 1990, **68**, 5804–5809.
85 L. Pintilie and I. Pintilie, *Mater. Sci. Eng., B*, 2001, **80**, 388–391.
86 Z. Lin, W. Cai, W. Jiang, C. Fu, C. Li and Y. Song, *Ceram. Int.*, 2013, **39**, 8729–8736.
87 C. Berglund and H. Braun, *Phys. Rev.*, 1967, **164**, 790.
88 Y. Jiang, X. Tang, Q. Liu, Q. Li and A. Ding, *Mater. Sci. Eng., B*, 2007, **137**, 304–309.
89 G. Khan, R. Das, N. Mukherjee and K. Mandal, *Phys. Status Solidi RRL*, 2012, **6**, 312–314.
90 J. W. Bennett and K. M. Rabe, *J. Solid State Chem.*, 2012, **195**, 21–31.
91 P. Poosanaas and K. Uchino, *Mater. Chem. Phys.*, 1999, **61**, 36–41.
92 A. Dogan, A. Prasadarao, K. Uchino, P. Poosanaas and S. Komarneni, *J. Electroceram.*, 1997, **1**, 105–111.
93 S. Shannigrahi and K. Yao, *Appl. Phys. Lett.*, 2005, **86**, 092901.
94 O. Beyer, C. von Korff Schmising, M. Luennemann, K. Buse and B. Sturman, *Opt. Express*, 2006, **14**, 1533–1540.
95 W. Warren, B. Tuttle and D. Dimos, *Appl. Phys. Lett.*, 1995, **67**, 1426–1428.
96 J.-K. Lee, C.-H. Kim, H.-S. Suh and K.-S. Hong, *Appl. Phys. Lett.*, 2002, **80**, 3593.
97 C. Brennan, *Ferroelectrics*, 1993, **150**, 199–208.
98 X. Lou, *J. Appl. Phys.*, 2009, **105**, 024101–024124.
99 S. A. Rodrigues, J. P. Silva, A. Khodorov, J. Martín-Sánchez, M. Pereira and M. Gomes, *Mater. Sci. Eng., B*, 2013, **178**, 1224–1229.
100 R. Guo, L. You, Y. Zhou, Z. S. Lim, X. Zou, L. Chen, R. Ramesh and J. Wang, *Nat. Commun.*, 2013, **4**, 1990.
101 F. Jermann and J. Otten, *J. Opt. Soc. Am. B*, 1993, **10**, 2085–2092.
102 V. Yarmarkin, B. Gol'tsman, M. Kazanin and V. Lemanov, *Phys. Solid State*, 2000, **42**, 522–527.
103 N. C. Giebink, G. P. Wiederrecht, M. R. Wasielewski and S. R. Forrest, *Phys. Rev. B: Condens. Matter Mater. Phys.*, 2011, **83**, 195326.
104 G. Yu, J. Gao, J. C. Hummelen, F. Wudl and A. J. Heeger, *Science*, 1995, **270**, 1789.
105 N. S. Sariciftci, L. Smilowitz, A. J. Heeger and F. Wudl, *Science*, 1992, **258**, 1474.
106 D. Veldman, O. Ipek, S. C. J. Meskers, J. Sweelssen, M. M. Koetse, S. C. Veenstra, J. M. Kroon, S. S. van Bavel, J. Loos and R. A. J. Janssen, *J. Am. Chem. Soc.*, 2008, **130**, 7721–7735.
107 D. Veldman, S. C. J. Meskers and R. A. J. Janssen, *Adv. Funct. Mater.*, 2009, **19**, 1939–1948.

108 C. L. Braun, *J. Chem. Phys.*, 1984, **80**, 4157.
109 K. Tvingstedt, K. Vandewal, A. Gadisa, F. L. Zhang, J. Manca and O. Inganas, *J. Am. Chem. Soc.*, 2009, **131**, 11819–11824.
110 M. Muntwiler, Q. Yang, W. A. Tisdale and X. Y. Zhu, *Phys. Rev. Lett.*, 2008, **101**, 196403.
111 S. S. Sun and N. S. Sariciftci, *Organic Photovoltaics: Mechanism, Materials, and Devices (Optical Engineering)*, 2005.
112 A. Pivrikas, H. Neugebauer and N. S. Sariciftci, *IEEE J. Sel. Top. Quantum Electron.*, 2010, **16**, 1746–1758.
113 K. Vandewal, K. Tvingstedt, A. Gadisa, O. Inganäs and J. V. Manca, *Nat. Mater.*, 2009, **8**, 904–909.
114 S. R. Cowan, N. Banerji, W. L. Leong and A. J. Heeger, *Adv. Funct. Mater.*, 2012, **22**, 1116–1128.
115 R. A. Marsh, J. M. Hodgkiss and R. H. Friend, *Adv. Mater.*, 2010, **22**, 3672–3676.
116 P. E. Keivanidis, T. M. Clarke, S. Lilliu, T. Agostinelli, J. E. Macdonald, J. R. Durrant, D. D. C. Bradley and J. Nelson, *J. Phys. Chem. Lett.*, 2010, **1**, 734–738.
117 I. A. Howard, R. Mauer, M. Meister and F. Laquai, *J. Am. Chem. Soc.*, 2010, **132**, 14866–14876.
118 J. M. Guo, H. Ohkita, H. Benten and S. Ito, *J. Am. Chem. Soc.*, 2010, **132**, 6154–6164.
119 W. L. Leong, S. R. Cowan and A. J. Heeger, *Adv. Energy Mater.*, 2011, **1**, 517–522.
120 R. Mauer, I. A. Howard and F. Laquai, *J. Phys. Chem. Lett.*, 2011, **2**, 1736–1741.
121 J. Kniepert, M. Schubert, J. C. Blakesley and D. Neher, *J. Phys. Chem. Lett.*, 2011, **2**, 700–705.
122 C. G. Shuttle, B. O'Regan, A. M. Ballantyne, J. Nelson, D. D. C. Bradley and J. R. Durrant, *Phys. Rev. B: Condens. Matter Mater. Phys.*, 2008, **78**, 113201.
123 S. R. Cowan, A. Roy and A. J. Heeger, *Phys. Rev. B: Condens. Matter Mater. Phys.*, 2010, **82**, 245207.
124 P. Wang, A. Abrusci, H. M. P. Wong, M. Svensson, M. R. Andersson and N. C. Greenham, *Nano Lett.*, 2006, **6**, 1789–1793.
125 X. Gong, M. Tong, F. G. Brunetti, J. Seo, Y. Sun, D. Moses, F. Wudl and A. J. Heeger, *Adv. Mater.*, 2011, **23**, 2272–2277.
126 Y. J. Park, I.-S. Bae, S. J. Kang, J. Chang and C. Park, *IEEE Trans. Dielectr. Electr. Insul.*, 2010, **17**, 1135–1163.
127 B. P. Neese, *Investigations of structure–property relationships to enhance the multifunctional properties of PVDF-based polymers*, The Pennsylvania State University, 2009.
128 M. Li, H. J. Wondergem, M.-J. Spijkman, K. Asadi, I. Katsouras, P. W. Blom and D. M. de Leeuw, *Nat. Mater.*, 2013, **12**, 433–438.
129 S. Horiuchi and Y. Tokura, *Nat. Mater.*, 2008, **7**, 357–366.
130 Z. Xiao, Q. Dong, P. Sharma, Y. Yuan, B. Mao, W. Tian, A. Gruverman and J. Huang, *Adv. Energy Mater.*, 2013, DOI: 10.1002/aenm.201300396.
131 S. W. Choi, J. R. Kim, Y. R. Ahn, S. M. Jo and E. J. Cairns, *Chem. Mater.*, 2007, **19**, 104–115.
132 Y. Yuan, P. Sharma, Z. Xiao, S. Poddar, A. Gruverman, S. Ducharme and J. Huang, *Energy Environ. Sci.*, 2012, **5**, 8558–8563.
133 Z. Hu, M. Tian, B. Nysten and A. M. Jonas, *Nat. Mater.*, 2008, **8**, 62–67.
134 A. V. Bune, V. M. Fridkin, S. Ducharme, L. M. Blinov, S. P. Palto, A. V. Sorokin, S. Yudin and A. Zlatkin, *Nature*, 1998, **391**, 874–877.
135 H. Sasabe, T. Furuno and T. Wada, *Mol. Cryst. Liq. Cryst.*, 1988, **160**, 281–296.
136 A. C. Rastogi, *J. Vac. Sci. Technol., B: Nanotechnol. Microelectron.: Mater., Process., Meas., Phenom.*, 2013, **31**, 04D112.
137 J. Kim, D.-S. Kim and S.-H. Lee, Solar cell using ferroelectric material (s), Google Patents, 6639143, 2003.
138 C. F. Pulvari, Efficient method and apparatus for converting solar energy to electrical energy, Google Patents, 4365106, 1982.
139 Y. Lu, Z. Xiao, Y. Yuan, H. Wu, Z. An, Y. Hou, C. Gao and J. Huang, *J. Mater. Chem. C*, 2013, **1**, 630–637.
140 A. Tada, Y. Geng, Q. Wei, K. Hashimoto and K. Tajima, *Nat. Mater.*, 2011, **10**, 450–455.
141 D. C. Coffey, B. W. Larson, A. W. Hains, J. B. Whitaker, N. Kopidakis, O. V. Boltalina, S. H. Strauss and G. Rumbles, *J. Phys. Chem. C*, 2012, **116**, 8916–8923.
142 K. S. Nalwa, J. A. Carr, R. C. Mahadevapuram, H. K. Kodali, S. Bose, Y. Chen, J. W. Petrich, B. Ganapathysubramanian and S. Chaudhary, *Energy Environ. Sci.*, 2012, **5**, 7042–7049.
143 K. Asadi, P. de Bruyn, P. W. Blom and D. M. de Leeuw, *Appl. Phys. Lett.*, 2011, **98**, 183301.
144 R. Naber, J. Massolt, M. Spijkman, K. Asadi, P. Blom and D. De Leeuw, *Appl. Phys. Lett.*, 2007, **90**, 113509.
145 R. Kalbitz, P. Frubing, R. Gerhard and D. Taylor, *Appl. Phys. Lett.*, 2011, **98**, 033303.
146 S. Horie, K. Ishida, S. Kuwajima, K. Kobayashi, H. Yamada and K. Matsushige, *Jpn. J. Appl. Phys.*, 2008, **47**, 1259.
147 P. Sharma, T. Reece, D. Wu, V. M. Fridkin, S. Ducharme and A. Gruverman, *J. Phys.: Condens. Matter*, 2009, **21**, 485902.
148 C. Dubourdieu, J. Bruley, T. M. Arruda, A. Posadas, J. Jordan-Sweet, M. M. Frank, E. Cartier, D. J. Frank, S. V. Kalinin and A. A. Demkov, *Nat. Nanotechnol.*, 2013, **8**, 748–754.
149 S. D. Stranks, G. E. Eperon, G. Grancini, C. Menelaou, M. J. Alcocer, T. Leijtens, L. M. Herz, A. Petrozza and H. J. Snaith, *Science*, 2013, **342**, 341–344.
150 G. Xing, N. Mathews, S. Sun, S. S. Lim, Y. M. Lam, M. Grätzel, S. Mhaisalkar and T. C. Sum, *Science*, 2013, **342**, 344–347.
151 C. Chang, V. H. Tran, J. Wang, Y.-K. Fuh and L. Lin, *Nano Lett.*, 2010, **10**, 726–731.
152 M. Glinchuk and A. Morozovskaya, *Phys. Status Solidi B*, 2003, **238**, 81–91.
153 R. Agrawal and H. D. Espinosa, *Nano Lett.*, 2011, **11**, 786–790.
154 Z. Zhao, V. Buscaglia, M. Viviani, M. T. Buscaglia, L. Mitoseriu, A. Testino, M. Nygren, M. Johnsson and P. Nanni, *Phys. Rev. B: Condens. Matter Mater. Phys.*, 2004, **70**, 024107.
155 D. D. Fong, G. B. Stephenson, S. K. Streiffer, J. A. Eastman, O. Auciello, P. H. Fuoss and C. Thompson, *Science*, 2004, **304**, 1650–1653.
156 F. Léonard and A. A. Talin, *Phys. Rev. Lett.*, 2006, **97**, 026804.
157 F. Léonard and A. A. Talin, *Nat. Nanotechnol.*, 2011, **6**, 773–783.
158 Y.-F. Lin and W.-B. Jian, *Nano Lett.*, 2008, **8**, 3146–3150.